

This article was downloaded by: [Graduate School]

On: 27 February 2013, At: 22:51

Publisher: Taylor & Francis

Informa Ltd Registered in England and Wales Registered Number: 1072954 Registered office: Mortimer House, 37-41 Mortimer Street, London W1T 3JH, UK



Journal of Adhesion Science and Technology

Publication details, including instructions for authors and subscription information:

<http://www.tandfonline.com/loi/tast20>

Assessments for impact of adhesive properties: modeling strength of metallic single lap joints

Wei Xu ^a & Yueguang Wei ^a

^a State Key Laboratory of Nonlinear Mechanics, Institute of Mechanics, Chinese Academy of Sciences, Beijing, 100190, P.R. China

Version of record first published: 13 Aug 2012.

To cite this article: Wei Xu & Yueguang Wei (2013): Assessments for impact of adhesive properties: modeling strength of metallic single lap joints, Journal of Adhesion Science and Technology, 27:1, 9-29

To link to this article: <http://dx.doi.org/10.1080/01694243.2012.701483>

PLEASE SCROLL DOWN FOR ARTICLE

Full terms and conditions of use: <http://www.tandfonline.com/page/terms-and-conditions>

This article may be used for research, teaching, and private study purposes. Any substantial or systematic reproduction, redistribution, reselling, loan, sub-licensing, systematic supply, or distribution in any form to anyone is expressly forbidden.

The publisher does not give any warranty express or implied or make any representation that the contents will be complete or accurate or up to date. The accuracy of any instructions, formulae, and drug doses should be independently verified with primary sources. The publisher shall not be liable for any loss, actions, claims, proceedings, demand, or costs or damages whatsoever or howsoever caused arising directly or indirectly in connection with or arising out of the use of this material.

Assessments for impact of adhesive properties: modeling strength of metallic single lap joints

Wei Xu* and Yueguang Wei

State Key Laboratory of Nonlinear Mechanics, Institute of Mechanics, Chinese Academy of Sciences, Beijing 100190, P.R. China

(Received 27 November 2011; final version received 14 February 2012; accepted 15 February 2012)

Adhesively bonded joints are widely used in a variety of industrial and engineering activities. Their overall strength is dependent on the properties of the adhesives. In the present research, assessments of adhesive properties were performed systematically through defining both strength mixity and energy rate mixity and using them to characterize the overall strength of metallic single lap joints. By means of the cohesive zone model, the adhesive strength mixity was defined as the ratio of the shear and tensile separation strength, and the energy rate mixity was defined as the ratio of the area below the shear cohesive curve and the area below the tensile cohesive curve. For each specified group of mixity parameters, corresponding to the properties of a specified adhesive, the overall strengths and the critical displacements of bonded joints were characterized. A series of strength and energy rate mixities were taken into account in the present calculations. A comparison of the present calculations with some existing experiments was carried out for both brittle and ductile adhesives. Finally, in the calculations presented here, damage initiation and evolution of the adhesive layer were also undertaken. The results showed that the overall strength of the joints was significantly depended on the adhesive properties, which were characterized by the strength and energy rate mixities of the adhesive. Furthermore, the shear adhesive stress components played a dominate role in both the damage initiation and evolution in the adhesives, which were also affected by the overlap length of the joints.

Keywords: finite element analysis; mixed-mode cohesive zone model; strength mixity; energy rate mixity; adhesively bonded joint

1. Introduction

Adhesively bonded joints (ABJ) are economical, practical and easy to make [1] and thus have been widely used to connect dissimilar materials in a variety of industries including civil engineering [2–4], automotive [5–7] and aircraft industries [8]. The strength evaluation and failure analysis of ABJ in various applications is an important topic. Accordingly, great efforts have been made in the finding efficient models for predicting the load-bearing capacity of ABJ, so as to design optimal joints with proper adhesives for practical requirements in engineering.

Much research in this area has previously been carried out on both analytically and theoretically topics. These can be grouped into two main categories. The first of these is based on stress analysis for both the shear and normal stress along the adhesive layer, being calculated

*Corresponding author. Email: xuwei@lnm.imech.ac.cn

to assess the load-bearing capacity of the joints [9–11]. The second category is based on a linear elastic fracture mechanical analysis, which appears to be a viable method to predict the overall strength of joints and has been investigated by other groups [12,13]. The adherends are considered to be elastic beams, which deform according to the classical Euler–Bernoulli beam theory, and the adhesive is regarded as a generalized spring medium [13]. In order to fully understand the failure mechanism of ABJ under complex conditions, a number of numerical models have been employed. In particular, by employing the commercially available Finite Element analysis codes (e.g. ABAQUS), many complicated issues have been investigated. Yang and Thouless [14] have developed a mode-dependence embedded process zone model and simulated the mixed-mode fracture of plastic deformable adhesive joints. The mode-I and mode-II fracture parameters adopted in the simulation have been obtained from their previous experimental tests. Similarly, Li et al. [15] have adopted the cohesive zone (CZ) approach to quantitatively predict the strengths and the mixed-mode failure mechanisms of the adhesively bonded composite joints. De Moura et al. [16,17] have also developed a mixed-mode CZ model with a trapezoidal shape traction–separation (T–S) law to predict the fracture behavior of adhesives. The results from these researchers have shown that the mode-dependence properties of adhesives play an important role in describing the overall strength of ABJ. As Yang and Thouless [14] have pointed out that the overall strength of a single lap-shear specimen is significantly larger than that of a T-peel specimen. The discrepancy of the overall strengths between the configurations is caused by the mode-dependence properties of the adhesives. Therefore, all the above quoted researchers have employed the mixed-mode numerical model based on an accurate description of the adhesives. Especially, by introducing of mixed-mode cohesive zone models (CZMs), the fracture behavior can be captured by several important cohesive parameters, which involves separation strengths and separation energies in shear and tensile directions.

Among the ABJ investigated by the above researchers, the single lap joint (SLJ) is a typical example of a mixed-mode configuration (shown in Figure 1(a)) to validate mixed-mode cohesive properties [14]. Because the failure of the SLJ is often accompanied by rotation of the overlap, both the normal and shear stresses along the adhesive will vary and re-distribute with the deformation of the SLJ [5]. Therefore, the material parameters in the tensile and shear directions would influence the failure behavior of SLJ together. Based on these considerations, some mixed-mode CZ models have been developed and employed in modeling the

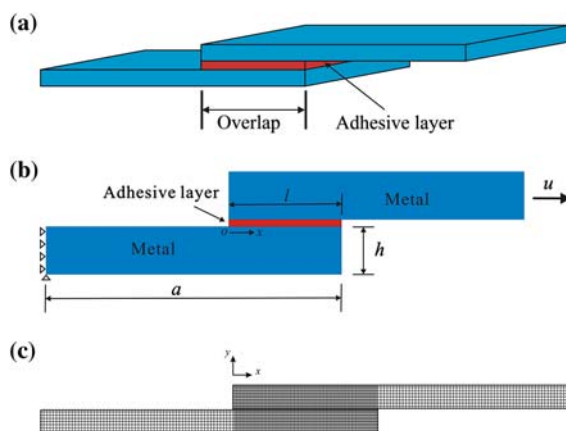


Figure 1. (a) Configuration of SLJ; (b) numerical model of the adhesive joint and (c) finite element mesh.

adhesives for joints [14,18]. The cohesive parameters utilized in the models were obtained from special tests. For example, the cohesive parameters of mode-I fracture were determined from double cantilever beam (DCB) tests [14,18,19]. Although in some numerical analyses of the SLJ, the adopted parameters of the mixed-mode CZ models were taken from related experimental measurements. However, the experimental data on the mechanical behavior of SLJ, which can be referred to, are very few. Early researchers working on the SLJ behavior were not systematical in their approach. For an example, there has not been an overall-assessment of the impact of adhesive properties, which should play a very important role in the strength and failure of SLJ systems.

In the present research, assessments of brittle and ductile adhesive properties were performed systematically through defining both strength mixity and energy rate mixity for adhesives and introducing the mixities to describe the interface debonding and the overall behavior of the SLJ. By using the CZ model, the adhesive strength mixity was defined as the ratio of shear to tensile separation strength, and the energy rate mixity was defined as the ratio of areas below the shear cohesive curve and below the tensile cohesive curve. For each specified group of the mixity parameters, corresponding to a particular adhesive, the overall strengths and the critical displacements of the bonded joint can be characterized. A series of strength and energy rate mixities were taken into account in the present calculations. Some comparisons with existing experiments were also investigated for both brittle and ductile adhesives. Finally, the damage initiation and evolution of adhesive layers was also investigated.

2. Model and simulation

In this section, a numerical model of the SLJ was built with the commercially available finite element method (FEM) code ABAQUS. All features used in the present calculations were built-in features of the FE code. For the present model, since the width of the adherends used for the joint was far larger than the thickness, the joints under tension can be treated as an elastic-plastic plane strain problem.

2.1. Computational model

Figure 1(b) depicts the computational model of the SLJ, which consists of two similar metallic adherends of thickness of h , having a typical value of 2 mm. The length of the adherends a was assigned the value of 120 mm. The adherends were connected by the adhesive layer of length l , which was also called an overlap length in this paper. The adherends were meshed using four-node quadrilateral plane strain elements, of which the total number was set at 2420 upon checking the convergence of the numerical results. Under uniaxial stretching, the joint was deformed under plane strain. In the numerical models, the left side of the joint was fixed in the horizontal direction, and the lower left corner was also fixed in the vertical direction. The model was loaded by means of an increasing displacement, and a uniform displacement of u was applied to the right side of the joint.

The metallic adherends were modeled as elastic-plastic solids, with their true stress-strain curves fitted using power-law hardening laws [20,21], as:

$$\sigma = \begin{cases} E\varepsilon & \varepsilon \leq \sigma^Y/E \\ \sigma^Y \left(\frac{\varepsilon}{\sigma^Y/E} \right)^N & \varepsilon > \sigma^Y/E \end{cases} \quad (1)$$

where E is the Young's modulus, N is the strain hardening exponent, and σ^Y is the yield strength. For the present model, the metallic adherends were assumed to be high-strength steel with the three material properties having the values of 200 GPa, 0.078 and 400 MPa, respectively.

2.2. Mixed-mode CZM

CZMs based on T-S laws were well suitable to describe the de-cohesion in composite structures. The CZMs require T-S relations for characterizing their constitutive laws. So far, considerable research has focused on the constitutive laws of CZMs and their applications [22]. It has been established that while the peak value and area of the T-S curve are vital for capturing the interface separation behavior, its precise shape is of less significance [23]. Consequently, for simplicity, the bilinear T-S law [22,24,25] shown in Figure 2 was selected for the present study. Built upon the bilinear CZM, the adhesive layer, also treated as interface between the two metallic adherends, was modeled with the CZ elements.

Figure 2 shows the T-S relation of the CZM, with Figure 2(a) and (b) giving the relationships in tensile and shear directions, respectively. To distinguish the tensile T-S law from the shear one, the superscript "n" represents the normal (or tensile) direction and "s" denote the shear direction. In Figure 2, u_m and u_c are the maximum and critical separation displacements, respectively, and T is the traction stress.

Since the maximum value of T^n is σ_m while that of $|T^s|$ is τ_m , the interfacial separation energy rates in the two directions can be expressed as:

$$\begin{aligned} \Gamma^n &= \int_0^{u_m^n} T^n du^n = \frac{1}{2} \sigma_m u_m^n \\ \Gamma^s &= \int_0^{u_m^s} T^s du^s = \frac{1}{2} \tau_m u_m^s \end{aligned} \quad (2)$$

As the loading is increased beyond a critical value, the interface begins to soften, and degrade, namely, the interface is now in the damaged (or softening) state. Typically, damage is initiated when a certain criterion is satisfied. In the present study, inspired by the bilinear law of Figure 2, the quadratic nominal stress criterion was adopted to characterize interfacial damage, described as:

$$\left(\frac{\langle T^n \rangle}{\sigma_m} \right)^2 + \left(\frac{T^s}{\tau_m} \right)^2 = 1 \quad (3)$$

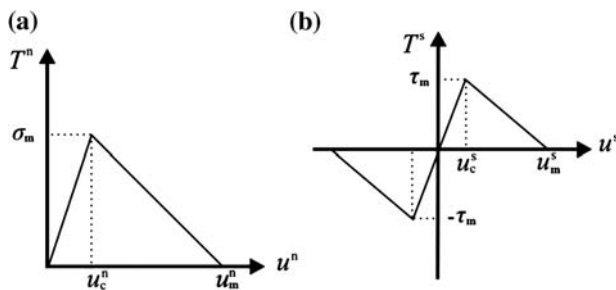


Figure 2. Typical bilinear T-S law of CZM: (a) T-S relation in tension and (b) T-S relation in shear.

where $\langle \cdot \rangle$ represents the Macaulay bracket defined by $\langle x \rangle = 1/2(x + |x|)$, with the usual interpretation that a pure compressive deformation or stress state does not initiate damage. The peak traction stresses σ_m and τ_m are termed the tensile and shear separation strengths, respectively.

It is assumed that interfacial damage occurs when Equation (3) is satisfied and a single damage variable D based on the total displacement jump Δ is introduced (i.e. $\Delta = \sqrt{\langle u^n \rangle^2 + (u^s)^2}$) [16,26], as:

$$D = \frac{\Delta_f(\Delta_{\max} - \Delta_c)}{\Delta_{\max}(\Delta_f - \Delta_c)} \quad (4)$$

where Δ_c and Δ_f denote the total displacement at damage initiation and complete failure. The quantity, Δ_f is determined by $\Delta_f = 2\Gamma/T_c^{\text{eff}}$ with T_c^{eff} denoting the effective traction at damage initiation (i.e. $T_c^{\text{eff}} = \sqrt{(T_c^n)^2 + (T_c^s)^2}$). In Equation (4), Δ_{\max} denotes the maximum total displacement experienced during the loading history.

Noting that Γ is the total separation energy of the adhesive, it can also be called the adhesive separation energy rate. Generally, Γ depends on the mode-mixity. In other words, the adhesive separation energy rate varies as a function of the mode-mixity. Thus, it could be termed the mixed-mode separation energy. In the present investigation, Γ was determined by the linear fracture criterion, which can be expressed as:

$$\frac{G^n}{\Gamma^n} + \frac{G^s}{\Gamma^s} = 1 \quad (5)$$

where G^n and G^s denote work done by the traction and its conjugate relative displacement in the tensile and shear directions, respectively. Γ^n and Γ^s refer to the critical separation energy rates required to cause failure in the tensile and shear directions, respectively, as defined in Equation (2). Consequently, the total adhesive separation energy rate can be determined by:

$$\Gamma = G^n + G^s \quad (6)$$

when Equation (5) is satisfied.

The adhesive layer was modeled with a single layer of four-node cohesive elements, which shared nodes with the neighboring elements in the upper and lower metallic adherends. In order to obtain better computational accuracy, the overlap region was densely meshed while sparse mesh was adopted in other regions as shown in Figure 1(c).

3. Influences of adhesive mode-mixities

3.1. General descriptions

The overall strength prediction and failure analysis of an ABJ are often implemented by accurate and reliable characterization of adhesive properties. As mentioned above, both the strength and the separation energy are two critical adhesive material parameters needed to determine the failure behavior of joints. The overall strength and failure behavior would exhibit the remarkable discrepancy under the single mode-I and single mode-II loadings [27], which results from that the adhesive properties in tensile direction are always different from those in shear direction. For some configurations such as DCB and T-peel specimens [14,19],

the tensile adhesive properties could have a more severe impact on the overall strength of the adhesive systems. By contrast, for other configurations, such as the SLJ [28], the shear adhesive properties would be more significant for the adhesive systems. For the purpose of characterizing the relationship between the tensile and shear adhesive properties, two types of mode-mixities are defined as follows:

$$\begin{aligned}\varphi &= \arctan\left(\frac{\tau_m}{\sigma_m}\right) \\ \Phi &= \arctan\left(\frac{\Gamma^s}{\Gamma^n}\right)\end{aligned}\quad (7)$$

where φ and Φ are called strength mixity and energy rate mixity, respectively. For a specified adhesive, the values of φ and Φ are constant values. Thus, in the present investigation, φ and Φ can be regarded as special adhesive properties. It should be noted that the two mixities are different from the phase angle ϕ defined in terms of the mode-I and mode-II energy release rate components at point of fracture, with the definition:

$$\phi = \arctan\left(\sqrt{\frac{G^s}{G^n}}\right)\quad (8)$$

which is used to characterize the relative proportions of shear to tensile deformations contributing to crack growth and the relationship between the mode-I and mode-II fracture behavior. Note, however, that the mixities defined in (7) are material characteristic parameters independent of the loading mode.

Combining Equations (5)–(8), the relationship between the energy rate mixity and the phase angle can be determined below, with the linkage of Γ and Γ^n :

$$\Gamma = \Gamma^n \frac{\tan \Phi (1 + \tan^2 \phi)}{\tan \Phi + \tan^2 \phi}\quad (9)$$

The total separation energy rate Γ normalized by Γ^n could be plotted as a function of loading mixity phase angle ϕ for selected energy rate mixity Φ , as shown in Figure 3(a); vari-

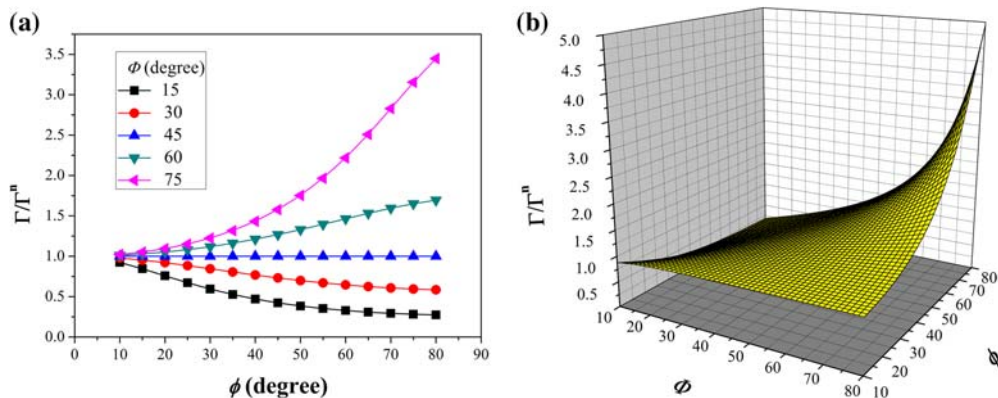


Figure 3. (a) Normalized total separation energy rate plots as a function of the loading mixity phase angle ϕ for selected energy rate mixities Φ . (b) Variation of normalized total separation energy rate with both the loading mixity phase angle and energy rate mixity.

ation of the normalized total separation energy rate is significantly influenced by Φ . With increasing ϕ , the normalized total separation energy rate increases when the Φ is larger than 45° , and also the increasing gradient is larger for a larger Φ . By contrast, the normalized total separation energy rate decreases when the Φ is less than 45° , and the decreasing gradient is larger for a smaller Φ . Noting that the failure mode would be simplified to the mode-independence when Φ is equal to 45° , namely, the normalized total separation energy rate keeps constant with the value of 1. In order to show the full view for the combined influence of energy rate mixity Φ and loading mode-mixity phase angle ϕ on the total separation energy rate, a 3D graph between the total separation energy rate and these two angles is plotted in Figure 3(b), which has a similar conclusion as Figure 3(a) shows.

3.2. Effect of strength mixity

Since the ductility of the adhesives can influence the strength and failure behavior of the ABJ [29–31], two types of adhesives were therefore considered in the present investigation: one was a ductile adhesive (i.e. Hysol EA 9361) and the other was a relatively brittle adhesive (i.e. Hysol EA 9321), which were also selected by the existing experiment [29]. The initial stiffnesses of the brittle and ductile adhesives were assigned the values of 7740 and 1340 MPa/mm, respectively, which were obtained from Refs. [29,33].

In this section, the influence of strength mixity of the adhesive was considered under the condition of similar separation energy rates with the values given in Table 1, taken from Ref. [29]. The separation energy rate components of the ductile adhesive were significantly larger than those of the brittle adhesive, which was the main discrepancy between the two types of adhesives.

It should be noted that the tensile separation strengths of the adhesives were assigned the same values of the yield strengths of the adhesives, namely, 4.23 MPa for the ductile adhesive and 21.99 MPa for the brittle adhesive. Strictly speaking in practice, the separation strength of adhesive is often larger than its yield strength [20], but the exact relation between the separation strength and yield strength is still unobtainable. Accordingly, the assumption of the tensile separation strength being equal to yield strength was adopted following previous research work [32]. For a specified adhesive, both the tensile and shear separation strengths should be two constant values. Unfortunately, the shear separation strength was not given in the original reference [29], which inspired us to explore the influence of the strength mixity of adhesives. As depicted in Table 2, the shear separation strength increases with the increasing adhesive strength mixity, according to Equation (7).

By employing the above adhesive parameters for the present model, the overall mechanical behavior of the SLJ model were obtained by FE calculations. Figures 4 and 5 show the load–displacement curves of the SLJ with the brittle and ductile adhesives, respectively, considering the influence of a series of strength mixities. It should be noticed that the exerted load is expressed in the form of F/h and the displacement is normalized by the adherend length a .

Table 1. Typical values of the separation energy rates for two types of adhesives [29].

Type	$\Gamma^n/\text{N mm}^{-1}$	$\Gamma^s/\text{N mm}^{-1}$
Brittle adhesive	0.45	0.90
Ductile adhesive	2.61	5.22

Table 2. Relation between the strength mixity and shear separation strength for two types of adhesives.

φ /degree	τ_m /MPa (brittle adhesive)	τ_m /MPa (ductile adhesive)
15	5.89	1.13
30	12.69	2.44
45	21.99	4.23
60	38.09	7.33
75	82.07	15.79

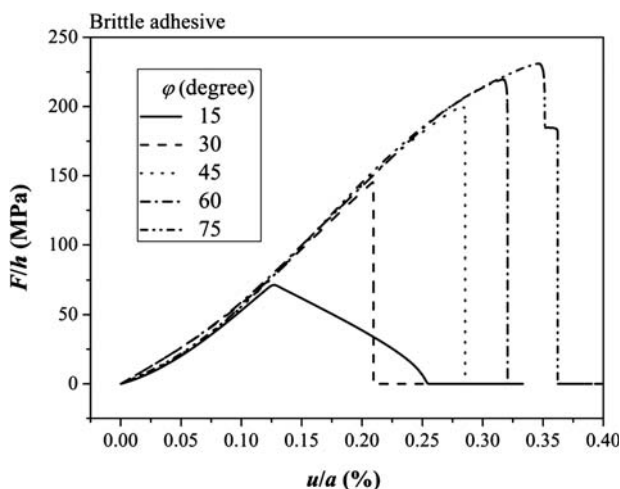


Figure 4. Load plotted as a function of displacement of SLJ with the brittle adhesive for the selected strength mixity angles.

Overall, both figures indicate that the load–displacement curves vary remarkably with the various strength mixities, which means the load-displacement relations were significantly influenced by the shear separation strength components. The curves will produce higher peaks for the larger strength mixities. Differently however, nearly all the curves in Figure 4 decreased dramatically in the declining stage except for the case of $\varphi = 15^\circ$. Because the total separation energy rate of the brittle adhesive is always relatively low, both the fracture process zone and the CZ are small. Consequently, the adhesive showed a brittle failure mode. It is worth mentioning that the adhesive corresponding to $\varphi = 15^\circ$ appeared as a ductile failure feature, which results from the following reason: it can be seen from Equation (2) that the characteristic lengths (u_m^n and u_m^s) of the CZ increase with decreasing separation strength when the separation energy rate is determined. For the case of $\varphi = 15^\circ$, the shear separation strength was low enough that the length of CZ was relatively large, which resulted in the ductile failure as depicted in Figure 4.

By contrast, nearly all the curves in Figure 5 decreased gradually, exhibiting a ductile failure feature. Similar to the special case in Figure 4, a special case is also seen in Figure 5, namely, the case corresponding to $\varphi = 75^\circ$. It shows the relatively brittle failure feature, which can be also explained by the reason given above.

In order to clearly show the influence of adhesive strength components on the overall strength of the joints, as presented in Figure 6, the peak load F_p was plotted as a function of the strength mixities for two types of adhesives. The results show the discrepancy between the brittle and ductile adhesives. Overall, the range of peak loads corresponding to the brittle adhesive was higher than that corresponding to the ductile adhesive except when the mixity angle was close to 90° . Besides, with the increasing strength mixity, the variations of the peak load for the two adhesives exhibited different trends. The rate of increase of the peak loads

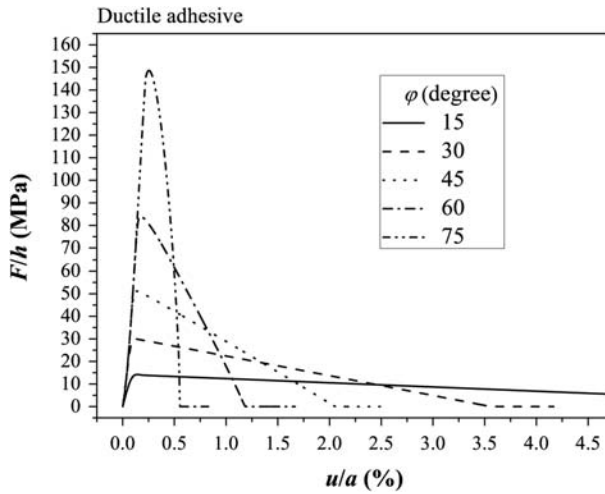


Figure 5. Load plotted as a function of displacement of SLJ with the ductile adhesive for the selected strength mixity angles.

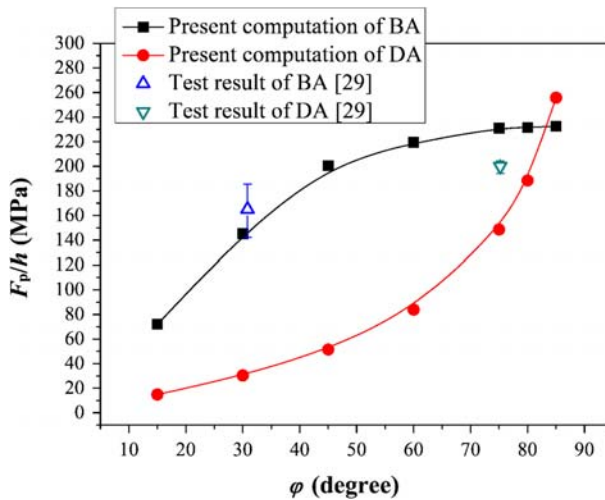


Figure 6. Peak load plotted as a function of strength mixity angle for both brittle (BA) and ductile adhesives (DA): comparison between the present model predictions with the experimental measurements [29].

for brittle adhesive slowed down and tended to a stable value, while that for the ductile adhesive, speeded up. Consequently, the peak load for the ductile adhesive exceeded that for the brittle adhesive when the mixity angle approached 90° .

For a purpose of checking the feasibility of the present numerical method, the existing experimental results [29] with the adoption of the same adhesives were compared with the computational predictions of the peak load. Here, the experimental strength mixity angle should have been calculated through the exact tensile and shear separation strengths. Unfortunately, the original reference [29] did not give the value of the shear separation strength. However, it could be estimated by using the equation $\tau_m = F_p/A$ with A denoting the lap area. It should be noted that the inaccuracy of the estimation by the equation $\tau_m = F_p/A$ may be caused by the rotation of the joint. However, the estimation by the equation was still adopted in the present investigation for the following reasons: on the one hand, the original reference (see, Ref. [29]) did not give the value of the shear separation strength. It was also very difficult to obtain the value through our literature search. Accordingly, though it is only a rough estimation, using the equation seems the only way to achieve the goal. On the other hand, the adherends adopted in the present model were made of high-strength steel, and thus, they had a much higher yield strength compared to that of the adhesive in the model. As a result, it can be predicted that the rotation of the joint is slight. Based on the above considerations, it was acceptable to use the equation for the estimation in the present investigation.

Generally, the deviations between the test results and predicted curves for both adhesives were not remarkable. However, compared with the deviation for the brittle adhesive, the deviation for the ductile adhesive was more notable. This was not only because of errors in both the experiment and in the original reference [29] but more significantly as a result of the assigned shear separation strength values for the test results. As previously pointed out, the values were determined by estimation through the equation $\tau_m = F_p/A$. The estimated value would be more accurate if the joint rotation was smaller. It can be predicted that the maximum rotation angle during the loading history would be smaller when the bondline was weaker under the condition of the same adherends. It can be seen in Figure 6 that the experimental peak load corresponding to the ductile case was obviously larger than that corresponding to the brittle case. Consequently, it was inferred that the maximum rotation angle for the ductile case was larger, which induced the larger deviation between the estimated value and the real value of the shear separation strength.

In the present investigation, the displacement corresponding to the peak load in Figure 4 was defined as the critical displacement u_c . Figure 7 plots the critical displacement as a function of strength mixity angle for both brittle and ductile adhesives. It is interesting to observe the similarity with Figure 6, which can be understood from the characteristic of the load-displacement curves of SLJ shown in Figures 4 and 5. In the rising stage of the curves, nearly all the curves appeared to have the same slope, which can be regarded as the stiffness of the joints. Obviously, the stiffness did not change with the strength mixity angle, which is caused not only by the linear elastic behavior of the interface prior to damage, but also because there is almost no plasticity. In the present investigation, since the adherends adopted in the present model were high-strength steels, they were stretched within the range of their linear elastic deformation, even though subjected to the peak load in the present model. Moreover, it can be seen that there was still only a small degree of nonlinearity in the load-displacement curves in Figure 4; this is due to the rotation of the joint and not due to the plasticity of the adherends. Based on the above reasons and inspired by the meaning of stiffness, it is reasonable to accept that the critical displacement will keep consistent with the peak load, as presented in Figure 7.

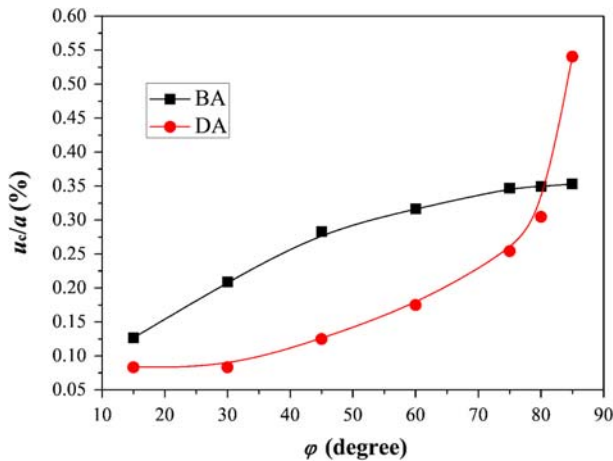


Figure 7. Critical displacement plotted as a function of strength mixity angle for both brittle and ductile adhesives.

3.3. Effect of separation energy rate mixity

In this section, the influence of adhesive separation energy rate components was considered with the introduction of the energy rate mixity. As presented in the above text, the mechanical behavior showed a significant discrepancy between the brittle and ductile adhesives, it is therefore necessary to consider the situations for the two adhesives separately.

In the present investigation, a series of separate energy rate mixities were obtained under the condition of same tensile separation energy rate Γ^m , taken from Table 1. According to the mixity definition in Equation (7), several shear separation energy rates can be obtained and are shown in Table 3. Previous researchers including both the experiments [28,31] and simulations [33,34] have pointed out that the separation strength and the separation energy rate have a combined effect on the strength of the ABJ. Thus, in the present simulation, the effect of the energy rate mixity should be taken into account together with the influence of the strength mixity.

The load-displacement relations of the SLJ subjected to the tensile loading can also be calculated, taking into account the two types of adhesives. The detailed load-displacement curves are shown in the Appendix. Based on the curves, the peak load could be obtained and plotted as a function of the energy rate mixity angle Φ for several strength mixities φ ; the cases of both brittle and ductile adhesives are shown in Figures 8 and 10, respectively.

For the brittle adhesive shown in Figure 8, the peak load generally increased as the energy rate mixity increased. However, the increasing tendency was significantly affected by

Table 3. Relation between the energy rate mixity and shear separation energy for two types of adhesives.

Φ /degree	$\Gamma^s/N \cdot \text{mm}^{-1}$ (brittle adhesive)	$\Gamma^s/N \cdot \text{mm}^{-1}$ (ductile adhesive)
15	0.12	0.70
30	0.26	1.51
45	0.45	2.61
60	0.78	4.52
75	1.68	9.74

the strength mixity effect. In detail, when the strength mixity angles were assigned relatively high values (e.g. $\varphi = 75^\circ$), the increased gradients of the peak load were large. In other words, with the increasing energy rate mixity, the peak load increased dramatically. In contrast, the peak load increased negligibly with increasing energy rate mixity when strength mixity angles were assigned relatively low values (e.g. $\varphi = 15^\circ$). The variation of critical displacement shown in Figure 9 had a similar tendency as that of peak load, which can be also understood by the reason presented in Section 3.2.

For the ductile adhesive, the situation was quite different. As shown in Figure 10, the variation of the peak loads was negligible as the energy rate mixity was increased. Especially when the strength mixity was considered large, namely in the range between 15° and 60° , the

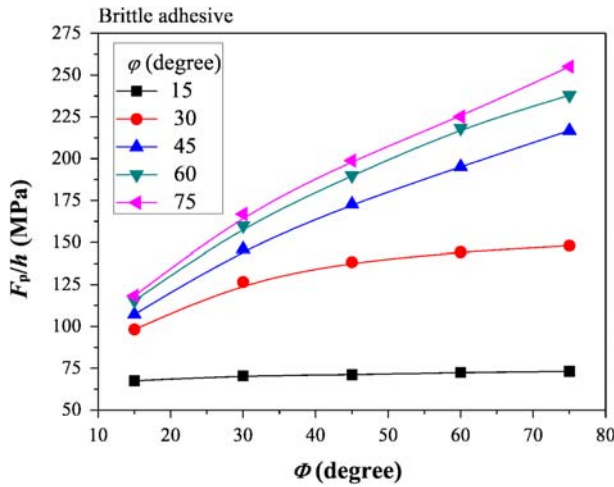


Figure 8. Peak load plotted as a function of energy rate mixity angle for various strength mixities, considering the category of brittle adhesive.

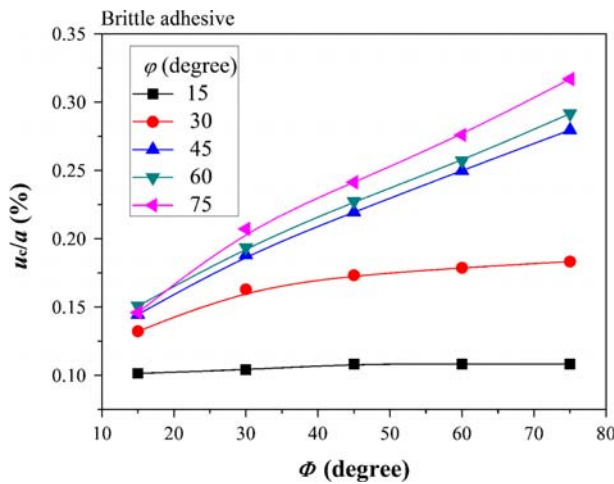


Figure 9. Critical displacement plotted as a function of energy rate mixity angle for various strength mixities, considering the category of brittle adhesive.

peak loads were almost unchanged with increasing energy rate mixity. Only a slight increase in the peak load was seen in the case of $\phi = 75^\circ$. Furthermore, as shown in Figure 11, the critical displacement corresponding to the ductile adhesive, generally had a similar tendency to the peak load, and the increasing tendency for some cases (i.e. $\phi = 45^\circ - 75^\circ$) was slightly more obvious than that of peak load shown in Figure 10, which could be explained based on the observation from Figure A2 in the Appendix. It can be seen in Figure A2 that when ϕ was small (e.g. $\phi = 15^\circ$ and 30°), there were two distinct stages in the curves, namely, the linear rise stage and linear decline stage. The peak points in the curves with various Φ values appeared superimposed. Consequently, there was little difference in the curves in Figures 10

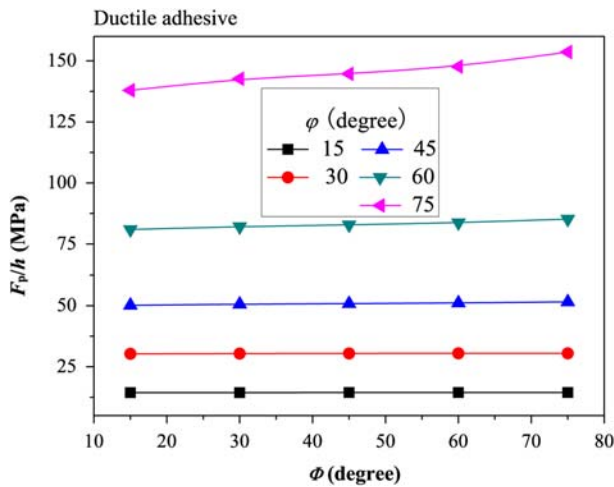


Figure 10. Peak load plotted as a function of energy rate mixity angle for various strength mixities, considering the category of ductile adhesive.

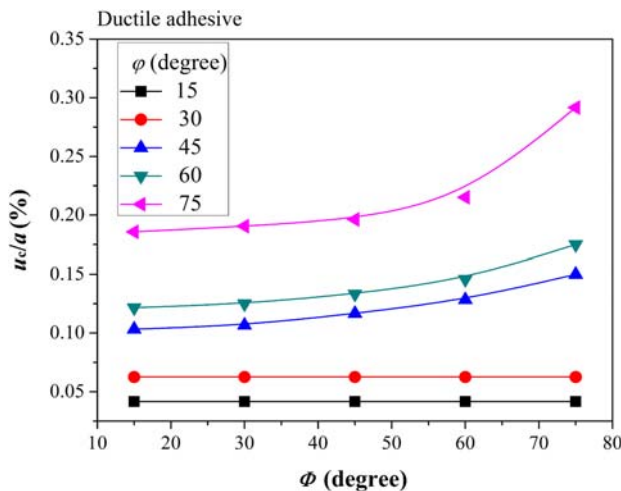


Figure 11. Critical displacement plotted as a function of energy rate mixity angle for various strength mixities, considering the category of ductile adhesive.

and 11 for the relatively smaller φ (i.e. 15° and 30°). However, when φ was relatively larger (e.g. $\varphi = 75^\circ$), the situation was quite different. It can be seen in Figure A2(e) that some curves (e.g. $\Phi = 15^\circ$ and 30°) exhibited two stages mentioned above, while other curves (e.g. $\Phi = 60^\circ$ and 75°) exhibited three stages including linear rise, nonlinear rise and a declining stage. As a result, the peak values of those curves were not the meeting points between the linear rise and declining stages. The existence of the nonlinear rise stage would induce the increased steps for the peak loads and critical displacements not to be equal, which in turn would cause the difference between Figures 10 and 11 for the higher values of φ .

In short, for the ductile adhesive, the overall strength of SLJ was not sensitive to the separation energy rate mixity even though the strength mixity was large, which may be due to the following reasons. The previous research has pointed out that the adhesive with the larger separation energy rate was able to distribute the load over a larger area [29]. In other words, the adhesive with the larger separation energy rate benefited and made full use of the load-bearing capacity of the adhesive layer. Thus, the overall strength of SLJ can be enhanced by increasing the separation energy rate from a small value to a relatively large value. However, when the separation energy rate increased further, with the load distribution being uniform along the adhesive layer, its load-bearing capacity attained saturation. After that, increasing the adhesive separation energy rate further will just increase the energy dissipation during bondline softening. In the present simulation, the separation energy rate of the ductile adhesive was profoundly larger than that of the brittle adhesive. Thus, increasing the adhesive separation energy rates, especially its shear component, will just increase the energy dissipation during the adhesive layer softening, without helping to enhance the load-bearing capacity. Noting that both strength and energy rate mixities were obtained from constant tensile fracture parameters in this paper, the larger values of mixities means larger shear fracture parameters. Based on the above analysis, the results given in Figure 10 can be understood.

4. Damage analysis

Note that all the loads increased to peak loads and then declined with increasing displacements as shown in Figures 4 and 5. Although the peak loads correspond neither to crack initiation nor to the onset of instability [14], the peak loads were generally regarded as the assessment values of the load-bearing capacity [1,29,31,35]. Thus, it is worth figuring out what happens to the adhesive layer when the load peaks. In order to find a reasonable answer, the damage analysis of the adhesive layer should be carried out considering the situation when the loads peak. In this section, both the brittle and ductile adhesives were considered with the separation energy rate components presented in Table 1. Additionally, the shear separation strengths of the brittle and ductile adhesives were 15.57 and 25.83 MPa, respectively, as obtained by inverse analysis from Figure 6, considering the case corresponding to adhesive thickness being equal to 1 mm in the original reference [29].

Equation (4) was employed to describe the damage level of the cohesive elements. The damage variable D increased monotonically from 0 (corresponding to damage initiation) to 1 (corresponding to total failure). Figure 12 plots the damage distribution along the adhesive layer when the peak loads were reached, with the horizontal axis denoting the position coordinate initiated at the left point “o” (see, Figure 1(b)). In order to obtain the influence not only from the adhesive type but also from the overlap length, the two adhesive types together with two overlap lengths were taken into account. It is interesting to note the main results. Firstly, the damage levels corresponding to ductile adhesive were more significant than those corresponding to brittle adhesive; this may be a result of the load distribution along the

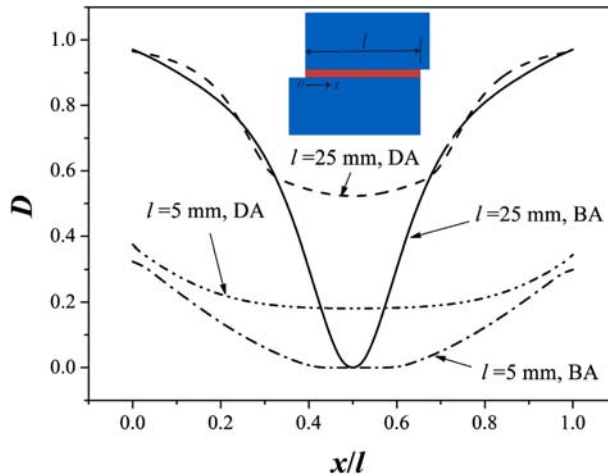


Figure 12. Damage variable distributions when the peak loads are reached, considering the influence of both the adhesive type and overlap length.

bondline. In Ref. [29], it is reported that the ductile adhesive was able to distribute the load over a large bonding area. Similar research [7] has also pointed out that adhesive shear stress distribution in SLJ with a ductile adhesive was more uniform than in the case of a brittle adhesive. Consequently, it is easy to understand why the damage distributions for ductile adhesives appeared more uniform when compared to the cases involving brittle adhesives. Moreover, although the SLJ for brittle adhesive reached its load-bearing peak, some areas near the midpoint of the overlap were not damaged; in other words, the damage variable for that area was zero. Secondly, all the curves in Figure 12 showed a higher damage level near both the extremities of the adhesive layer. This was reasonable since both the tensile and shear stress components were relatively high near the extremities of the adhesive layer [28,36]. Finally, the influence of the overlap length was clear. The damage distribution for the short overlap length (i.e. $l = 5\text{ mm}$) was more uniform. By contrast, the variation of the damage distribution for the long overlap length (i.e. $l = 25\text{ mm}$) was much more severe. In other words, the discrepancy between the peak and the low values of the damage variable along the overlap was considerable for the long overlap length. Furthermore, when the SLJ reached its peak load, the damage level along the adhesive layer corresponding to long overlap length was higher. It implied that the load-bearing capacity of the adhesive layer with a short overlap length was not made full use of in comparison with long overlap length.

Although it is apparent that the shear adhesive stress component plays a leading role in the damage process of SLJs, the effect of the shear stress component needs to be quantitatively explored. Considering that both the shear and tensile stress components contributed to the damage initiation in adhesive as suggested by Equation (3), the proportions of the each stress component is still unknown. In particular, the contribution of the shear stress component to the damage initiation should be clarified. Accordingly, Figure 13 plots the contribution distribution of shear stress component to the damage initiation in the adhesive layer, considering the influence of both the adhesive type and the overlap length. The contribution of the shear stress component to damage initiation can be expressed in terms of $(T^s/\tau_m)^2$. Noting that the mid region of bondline for the case with the brittle adhesive and $l = 25\text{ mm}$ was not damaged (i.e. $D = 0$) as shown in Figure 12; thus, the part of the curve for this case in Figure 13 (i.e. the region between the two highlighted points) would not represent the

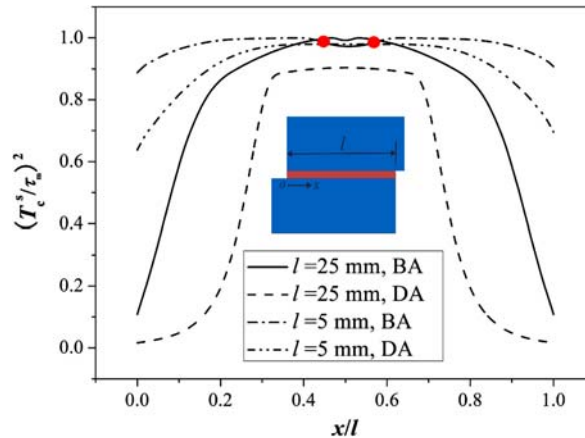


Figure 13. Contribution distribution of shear stress component to the damage initiation of the adhesive layer, considering the influence of both the adhesive type and the overlap length.

contribution to the damage initiation. Moreover, according to Eq. (3), the potential contribution of the tensile stress component to damage initiation can be given by $1 - (T^s/\tau_m)^2$.

As shown in Figure 13, the contribution of the shear stress component was affected by both the adhesive type and the overlap length. On the one hand, the contribution corresponding to brittle adhesive was larger than that corresponding to ductile adhesive. On the other hand, the contribution with respect to short overlap length (i.e. $l = 5$ mm) was large and uniform. Furthermore, all the curves suggested that the contribution from the shear stress component appeared relatively low level near the extremities of the overlap. In other words, the contribution from the tensile stress component would be relatively higher in those areas. Despite this, the influence of tensile component became relatively noticeable near the extremities, the shear component still played a dominant role in that area for the case of short overlap length because the minimum value of $(T^s/\tau_m)^2$ was still more than 0.6 for both adhesive types.

5. Concluding remarks

In summary, assessments for the impact of adhesive properties have been performed systematically through defining both strength mixity and energy rate mixity for adhesives and using them to characterize the overall behavior of metallic SLJs. Both the overall strengths and the critical displacements of the joint have been characterized. A series of the strength and energy rate mixities that describe the various adhesive properties have been taken into account in the present calculations. Some comparisons of calculated results with existing experiments have been carried out for both brittle and ductile adhesives. The damage initiation and evolution of the adhesive layer have also been analyzed. The present results have shown that the overall strengths of the joints are significantly dominated by the adhesive properties, which can be characterized by the strength and energy rate mixities. Furthermore, the shear adhesive stress component played a dominant role in both the damage initiation and evolution in the adhesives, which were also considerably affected by the overlap length of the joints.

It is worth mentioning that, in the present research, some issues are still not resolved and should be considered in future. Firstly, the adherends for the present model were high-strength steel with high yield strength, and plastic deformation of the adherends probably did not occur. Further work considering other metallic adherends susceptible to plastic deformation is needed. Secondly, the failure mode of the joint was another key issue. In fact,

depending on the loading and boundary conditions, for the metallic ABJ, there may be two different failure modes as follows: (a) adhesion failure occurring at the interfacial surface between the adherends (i.e. metallic adherends in the present study) and the adhesive layer and (b) cohesion failure occurring in the adhesive layer [37]. However, in the present model, only the damage of the cohesion failure was carried out and the other failure mode was not considered. Proper failure criteria should be implemented in the models for the purpose of estimating the failure mode in the adhesive bonding systems. Thirdly, generally speaking, the adhesive thickness could influence the strength of the ABJ; previous researchers have studied the influence and have reported their results [29]. Increasing the adhesive thickness would increase the total fracture energy, which consists of intrinsic cohesive energy (i.e. fracture toughness) and plastic dissipation energy. Since the intrinsic cohesive energy of the adhesive is constant, the variation of the total fracture energy would be induced by the variation of the plastic dissipation energy. However, the present investigation was aimed at assessing the impact of a series of adhesive properties, which played a role in the SLJ; hence, the influence of various adhesive thicknesses was not considered. The exact relationship between the total fracture energy and the thickness of the adhesive layer would be investigated in our future work.

Acknowledgements

This work was supported by the National Natural Science Foundation of China (11021262, 10932011 and 90816004) and MOST of China through Grant 2012CB937500.

References

- [1] Kahraman R, Sunar M, Yilbas B. Influence of adhesive thickness and filler content on the mechanical performance of aluminum single-lap joints bonded with aluminum powder filled epoxy adhesive. *Journal of Materials Processing Technology*. 2008;205:183–89.
- [2] Wu ZS, Yuan H, Niu HD. Stress transfer and fracture propagation in different kinds of adhesive joints. *Journal of Engineering Mechanics-ASCE*. 2002;128:562–73.
- [3] Dai JG, Ueda T, Sato Y. Development of the nonlinear bond stress-slip model of fiber reinforced plastics sheet-concrete interfaces with a simple method. *Journal of Composites for Construction*. 2005;9:52–62.
- [4] Ascione F. Mechanical behaviour of FRP adhesive joints: A theoretical model. *Composites Part B-Engineering*. 2009;40:116–24.
- [5] Grant LDR, Adams RD, da Silva LFM. Experimental and numerical analysis of single-lap joints for the automotive industry. *International Journal of Adhesion and Adhesives*. 2009;29:405–13.
- [6] Grant LDR, Adams RD, da Silva LFM. Effect of the temperature on the strength of adhesively bonded single lap and T joints for the automotive industry. *International Journal of Adhesion and Adhesives*. 2009;29:535–42.
- [7] Loureiro AL, da Silva LFM, Sato C, Figueiredo MAV. Comparison of the mechanical behavior between stiff and flexible adhesive joints for the automotive industry. *Journal of Adhesion*. 2010;86:765–87.
- [8] Higgins A. Adhesive bonding of aircraft structures. *International Journal of Adhesion and Adhesives*. 2000;20:367–76.
- [9] Tong L. Bond strength for adhesive-bonded single-lap joints. *Acta Mechanica*. 1996;117:101–13.
- [10] Luo QT, Tong LY. Analytical solutions for nonlinear analysis of composite single-lap adhesive joints. *International Journal of Adhesion and Adhesives*. 2009;29:144–54.

- [11] da Silva LFM, das Neves PJC, Adams RD, Spelt JK. Analytical models of adhesively bonded joints-Part I: Literature survey. *International Journal of Adhesion and Adhesives*. 2009;29:319–30.
- [12] Hafiz TA, Wahab MMA, Crocombe AD, Smith PA. Mixed-mode fracture of adhesively bonded metallic joints under quasi-static loading. *Engineering Fracture Mechanics*. 2010;77:3434–45.
- [13] Alfredsson KS, Högberg JL. Energy release rate and mode-mixity of adhesive joint specimens. *International Journal of Fracture*. 2007;144:267–83.
- [14] Yang QD, Thouless MD. Mixed-mode fracture analyses of plastically-deforming adhesive joints. *International Journal of Fracture*. 2001;110:175–87.
- [15] Li S, Thouless MD, Waas AM, Schroeder JA, Zavattieri PD. Mixed-mode cohesive-zone models for fracture of an adhesively bonded polymer-matrix composite. *Engineering Fracture Mechanics*. 2006;73:64–78.
- [16] De Moura MFSF, Campilho RDSG, Goncalves JPM. Mixed-mode cohesive damage model applied to the simulation of the mechanical behavior of laminated composite adhesive joints. *Journal of Adhesion Science and Technology*. 2009;23:1477–91.
- [17] De Moura MFSF, Goncalves JPM, Chousal JAG, Campilho RDSG. Cohesive and continuum mixed-mode damage models applied to the simulation of the mechanical behaviour of bonded joints. *International Journal of Adhesion and Adhesives*. 2008;28:419–26.
- [18] Sun C, Thouless MD, Waas AM, Schroeder JA, Zavattieri PD. Rate effects for mixed-mode fracture of plastically-deforming, adhesively-bonded structures. *International Journal of Adhesion and Adhesives*. 2009;29:434–43.
- [19] Li S, Thouless MD, Waas AM, Schroeder JA, Zavattieri PD. Use of a cohesive-zone model to analyze the fracture of a fiber-reinforced polymer-matrix composite. *Composites Science and Technology*. 2005;65:537–49.
- [20] Pardoën T, Ferracin T, Landis CM, Delannay F. Constraint effects in adhesive joint fracture. *Journal of the Mechanics and Physics of Solids*. 2005;53:1951–83.
- [21] Xu W, Wei Y. Strength analysis of metallic bonded joints containing defects. *Computational Materials Science*. 2012;53:444–50.
- [22] Chandra N, Li H, Shet C, Ghonem H. Some issues in the application of cohesive zone models for metal-ceramic interfaces. *International Journal of Solids and Structures*. 2002;39:2827–55.
- [23] Freund LB, Suresh S. *Thin Film Materials: Stress, Defect Formation and Surface Evolution*. Cambridge: Cambridge University Press; 2003.
- [24] Ghosh S, Ling Y, Majumdar B, Kim R. Interfacial debonding analysis in multiple fiber reinforced composites. *Mechanics of Materials*. 2000;32:561–91.
- [25] Li H, Chandra N. Analysis of crack growth and crack-tip plasticity in ductile materials using cohesive zone models. *International Journal of Plasticity*. 2003;19:849–82.
- [26] Balzani C, Wagner W. An interface element for the simulation of delamination in unidirectional fiber-reinforced composite laminates. *Engineering Fracture Mechanics*. 2008;75:2597–615.
- [27] Balzani C, Wagner W, Wilckens D, Degenhardt R, Büsing S, Reimerdes HG. Adhesive joints in composite laminates—combined numerical/experimental estimate of critical energy release rates. *International Journal of Adhesion and Adhesives*. 2012;32:23–38.
- [28] da Silva LFM, Critchlow GW, Figueiredo MAV. Parametric study of adhesively bonded single lap joints by the taguchi method. *Journal of Adhesion Science and Technology*. 2008;22:1477–94.
- [29] da Silva LFM, Rodrigues TNSS, Figueiredo MAV, de Moura MFSF, Chousal JAG. Effect of adhesive type and thickness on the lap shear strength. *Journal of Adhesion*. 2006;82:1091–115.
- [30] Banea MD, Silva LFM. Mechanical characterization of flexible adhesives. *Journal of Adhesion*. 2009;85:261–85.
- [31] da Silva LFM, Carbas RJC, Critchlow GW, Figueiredo MAV, Brown K. Effect of material, geometry, surface treatment and environment on the shear strength of single lap joints. *International Journal of Adhesion and Adhesives*. 2009;29:621.

- [32] Rudawska A. The influence of adhesive constitutive parameters in cohesive zone finite element models of adhesively bonded joints. *International Journal of Adhesion and Adhesives*. 2010;30:574.
- [33] Gustafson PA, Waas AM. The roles of toughness and cohesive strength on crack deflection at interfaces. *International Journal of Solids and Structures*. 2009;46:2201–15.
- [34] Parmigiani JP, Thouless MD. Adhesive joint strength of hybrid assemblies: Titanium sheet-composites and aluminium sheet-composites—Experimental and numerical verification. *Journal of the Mechanics and Physics of Solids*. 2006;54:266–87.
- [35] de Morais AB, Pereira AB, Teixeira JP, Cavaleiro NC. Strength of epoxy adhesive-bonded stainless-steel joints. *International Journal of Adhesion and Adhesives*. 2007;27:679–86.
- [36] You M, Yan ZM, Zheng XL, Yu HZ, Li Z. A numerical and experimental study of adhesively bonded aluminium single lap joints with an inner chamfer on the adherends. *International Journal of Adhesion and Adhesives*. 2008;28:71–6.
- [37] Xu W, Wei Y. Strength and interface failure mechanism of adhesive joints. *International Journal of Adhesion and Adhesives*. 2012;34:80.

Appendix

In Section 3.3, the peak loads and the corresponding critical displacements were obtained for the underlying load–displacement relations of SLJ subjected to the tensile loading. They can be calculated with various adhesive parameters. Figure A1 shows the load-displacement curves of SLJ with the brittle adhesive for the selected energy rate mixity angles, considering five selected strength mixity angles: (a) 15°, (b) 30°, (c) 45°, (d) 60°, and (e) 75°, while those for the ductile adhesive are presented in Figure A2.

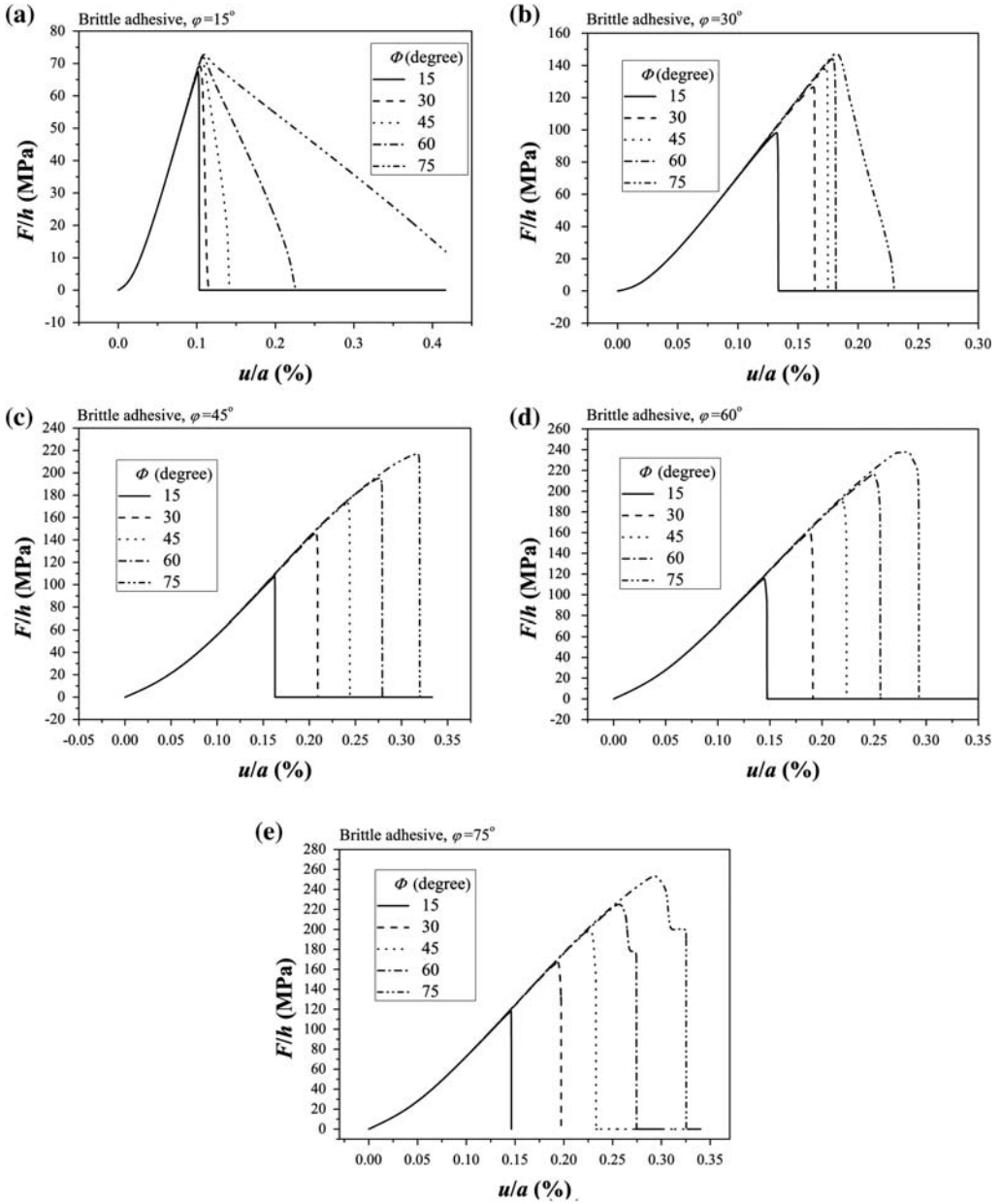


Figure A1. Load plotted as a function of displacement of SLJ with the brittle adhesive for the selected energy rate mixity angles, considering five selected strength mixity angles: (a) 15° ; (b) 30° ; (c) 45° ; (d) 60° ; and (e) 75° .

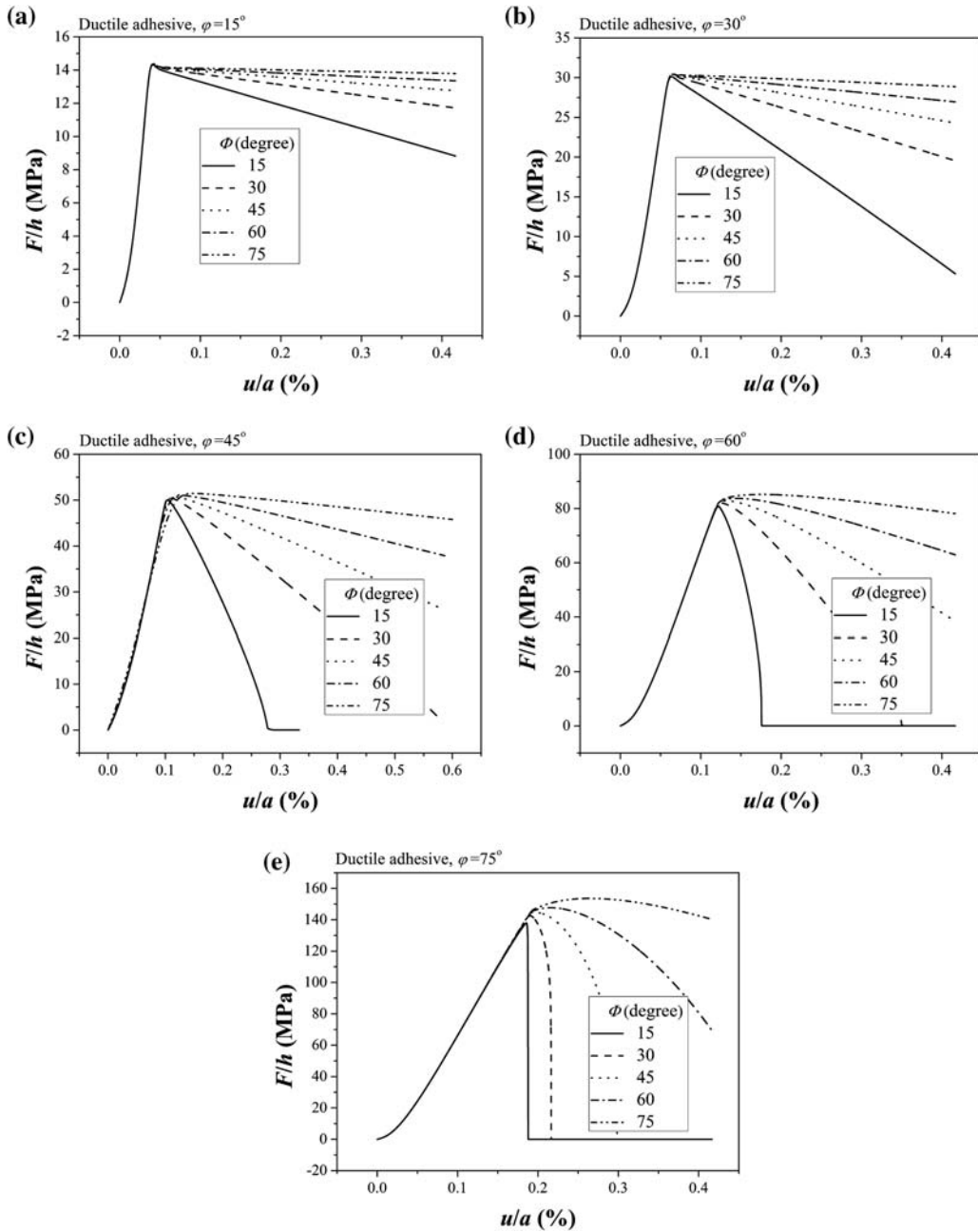


Figure A2. Load plotted as a function of displacement of SLJ with the ductile adhesive for the selected energy rate mixity angles, considering five selected strength mixity angles: (a) 15° ; (b) 30° ; (c) 45° ; (d) 60° ; and (e) 75° .